Available online at www.sciencedirect.com
ScienceDirect
Journal of Sound and Vibration 310 (2008) 902–922
JOURNAL OF SOUND AND VIBRATION
www.elsevier.com/locate/jsvi

Multimodal method for scattering of sound at a sudden area expansion in a duct with subsonic flow

G. Kooijman[a,*], P. Testud[b], Y. Aurégan[c], A. Hirschberg[a]

[a]*Department of Applied Physics, Fluid Dynamics Laboratory, Eindhoven University of Technology, P.O. Box 513, 5600 MB, Eindhoven, The Netherlands*
[b]*LaMSID, UMR CNRS EDF 2832, EDF R&D, 1 Avenue de Général de Gaulle, 92141 Clamart Cedex, France*
[c]*Laboratoire d'Acoustique de l'Université du Maine, Avenue Olivier Messiaen 72085, Le Mans, Cedex 9, France*

Received 13 March 2007; received in revised form 11 July 2007; accepted 13 August 2007
Available online 29 September 2007

Abstract

The scattering of sound at a sudden area expansion in a duct with subsonic mean flow has been modelled with a multimodal method. Technological applications are for instance internal combustion engine exhaust silencers and silencers in industrial duct systems. Both two-dimensional (2D) rectangular and 2D cylindrical geometry and uniform mean flow as well as non-uniform mean flow profiles are considered. Model results for the scattering of plane waves in case of uniform flow, in which case an infinitely thin shear layer is formed downstream of the area expansion, are compared to results obtained by other models in literature. Generally good agreement is found. Furthermore, model results for the scattering are compared to experimental data found in literature. Also here fairly good correspondence is observed. When employing a turbulent pipe flow profile in the model, instead of a uniform flow profile, the prediction for the downstream transmission- and upstream reflection coefficient is improved. However, worse agreement is observed for the upstream transmission and downstream reflection coefficient. On the contrary, employing a non-uniform jet flow profile, which represents a typical shear layer flow downstream of the expansion, gives worse agreement for the downstream transmission- and the upstream reflection coefficient, whereas prediction for the upstream transmission and downstream reflection coefficient improves.

1. Introduction

In duct systems carrying mean flow, flow separation occurs at abrupt area expansions. Interaction between sound and vorticity disturbances in the shear layer, formed downstream of the expansion, can occur, possibly leading to sound absorption. This is in particular of interest in technical applications as internal combustion engine exhaust silencers and silencers in industrial duct systems.

Probably the most extensive experimental work on this topic is that of Ronneberger [1]. He presented results for both magnitude and phase of the reflection—as well as transmission coefficients of the acoustic plane pressure waves at an area expansion in a cylindrical duct with anechoic termination.

*Corresponding author. Tel.: +31 40 2473154.
E-mail address: g.kooijman@tue.nl (G. Kooijman).

0022-460X/$ - see front matter © 2007 Elsevier Ltd. All rights reserved.
doi:10.1016/j.jsv.2007.08.008

The effect on the acoustic propagation in ducts with area discontinuities in absence of mean flow is solved by e.g. Miles [2] and Kergomard and Garcia [3]. Early models to describe the acoustical properties of an area expansion in a duct with mean flow are that of Ronneberger [4] and Alfredson and Davies [5]. Here, in a low-frequency plane wave approximation, one-dimensional (1D) linearized equations for the conservation of mass, momentum and energy are applied to a control volume around the area expansion. Dissipation is accounted for by entropy fluctuations, associated with the formation of vortices in the mixing region downstream of the expansion, which is thus included in the control volume. Alfredson and Davies [5] compared theoretical prediction and experimental data for the reflection coefficient up to a Mach number of 0.15. Reasonable agreement was found. Ronneberger [4] compared predicted and measured results for the reflection coefficient up to Mach numbers of 0.6, but also here only good agreement was obtained for Mach numbers below ~0.15. Cummings [6] proposed a similar model, in which scattering is assumed to occur in the control volume, where the flow has not yet expanded. However, energy losses due to the vorticity are now accounted for by entropy waves downstream of the control volume. Comparison with Ronneberger's experimental results yielded better agreement for the higher Mach numbers. Furthermore, in a later correspondence [7] he concluded that entropy fluctuations need not to be taken into account as they are of secondary importance and probably are negligible compared to higher-order modes and shear flow effects. All of the above-mentioned models lack the effects of higher-order modes as they are low-frequency, plane wave approximations.

Lambert and Steinbrueck [8] proposed a low-frequency, low Mach number model on the basis of the statement that the magnitude of the reflection coefficient at an area expansion is only Mach number dependent, whereas its phase is only frequency dependent. The magnitude is calculated from applying conservation equations to a control volume around the area expansion, in which the mean flow has expanded. The phase is calculated from an equivalent end correction for no mean flow [9]. Davies [10] proposed a similar model, in which the phase is calculated from either an equivalent end correction or by including higher-order modes in the matching of the ducts upstream and downstream of the area expansion. The use of an equivalent end correction for the phase of the reflection coefficient was extended to higher frequencies by Peat [11], who also compared results of the analytical model with a finite-element method. It has to be noted here, that the, in these models, assumed dependency of magnitude and phase of the reflection coefficient on only Mach number, respectively, only frequency is actually in contradiction with for example experimental results of Ronneberger [1] and theoretical results of Boij and Nilsson [12] (see also below). Also, in the closely related problems of reflection at an open pipe with mean flow and scattering at an orifice in a pipe with mean flow the magnitude and phase is found to be dependent on both Mach number and frequency. This was shown experimentally by Peters [13,14] and Allam and Åbom [15] and theoretically by Munt [16,17], Rienstra [18] and Cargill [19] for the open pipe, and by e.g. Hofmans [20] and Testud [21] for the orifice.

Aurégan [22,23] presented a simplified multimodal model for the aero-acoustic behaviour of a sudden area expansion at low frequency in a cylindrical duct. The uniform mean flow was considered to remain unexpanded after the area discontinuity, giving an infinitely thin shear layer. The effect of entropy fluctuations due to mixing downstream of the expansion is not accounted for. The acoustic pressure and radial velocity field downstream of the expansion was expanded into six modes assuming a prescribed form [24]: a plane wave mode and a mode accounting for higher-order effects in either direction of propagation, and two hydrodynamic modes. Subsequently, applying continuity of mean acoustic pressure and volume flux and a Kutta condition at the area discontinuity gave the acoustic behaviour. A favourable comparison of the predicted magnitude of the reflection coefficient with the experimental results of Ronneberger [1] was shown. Earlier, Nilsson and Brander [25,26] employed a full modal analysis for the same configuration of an infinitely thin shear layer.

An alternative method was given by Dupère and Dowling [27]. They described the interaction of the shear layer with the sound field by means of an acoustic analogy, in which the shear layer acts as a source/sink term in the wave equation in the downstream duct. In their model the Mach number is very low and the shear layer is assumed to be thick, such that hydrodynamic instability does not occur.

Recently, Boij and Nilsson [12] presented a model for the scattering at an area discontinuity in a rectangular two-dimensional (2D) duct carrying uniform mean flow. Also in this model the flow is considered to remain unexpanded after the area discontinuity. Higher-order acoustic modes and hydrodynamic modes are taken into account, and the problem is solved with the Wiener–Hopf technique with application of a Kutta

condition at the edge of the area discontinuity. A favourable comparison for the scattering coefficients with experimental results of Ronneberger [1,4] is made. For this purpose a normalization of the Helmholtz number for both rectangular and cylindrical ducts is proposed. In a latter paper [28] they addressed the issue of (in)stability of the vortex sheet. As the mean flow is assumed to be uniform and continues unaltered after the expansion, an infinitely thin shear layer is formed. Such a vortex sheet is always unstable. However, a real shear layer with finite thickness becomes stable for sufficiently large Strouhal numbers. This is seen for instance for the hyperbolic-tangent profile, of which the (in)stability was investigated by Michalke [29]. Boij and Nilsson accounted for this physical effect by suppressing the hydrodynamic instability mode for higher Strouhal numbers. This was done by introducing a gradually relaxed Kutta condition at the edge, with empirical coefficients as to give a better fit with experimental results for the downstream reflection coefficient. They reported that the effect of the relaxed Kutta condition on the downstream transmission coefficient is negligible. In the same paper they also calculate the absorption of energy at the area expansion, either accounting for the expansion of the flow downstream of the area discontinuity or not accounting for it.

In this paper, sound scattering at an area expansion in a duct with flow is investigated analytically with a model based on multimodal analysis of the acoustic field, see e.g. Auregan et al. [30], Kooijman [31,32], Testud [21], and Leroux [33]. As in the simplified multimodal model of Aurégan [22,23] and in the model of Boij and Nilsson [12] the contribution of entropy waves due to the expansion of the flow downstream of the area discontinuity is neglected here. Unlike the alternative models mentioned above, this model allows for a non-uniform flow profile, such that the thickness of the shear layer can be included. This model does not need the relaxed Kutta condition used by Boij and Nilsson. First the multimodal method will be discussed. Subsequently, results for the scattering in case of an infinitely thin shear layer will be compared to results of Boij and Nilsson's model [12] and Aurégan's model [22,23]. Here, in the light of the Helmholtz number scaling proposed by Boij and Nilsson as mentioned above, both calculations in 2D Cartesian and 2D cylindrical geometry are presented and compared. Finally, model results are compared with the experimental data of Ronneberger [1]. Specifically, the effect of taking into account the non-uniformity of the flow (thickness of the shear layer) is investigated.

2. Multimodal analysis

The multimodal analysis method applied to the sudden area expansion in a duct with flow will be discussed for both uniform flow (infinitely thin shear layer) and non-uniform flow. Equations will in first instance be derived for the case of 2D rectangular geometry. At the end the extension to 2D cylindrical geometry, which involves only minor changes, is given.

2.1. Non-uniform flow

Consider a sudden area expansion in a 2D rectangular duct (Fig. 1). The geometrical configuration can be split into a duct at $x<0$ with height h_1 and a duct at $x>0$ with height h_2. The two are indicated in the figure

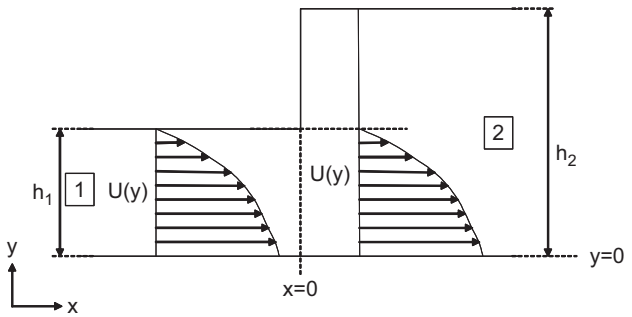

Fig. 1. Area expansion in a two-dimensional rectangular duct. Configuration is split in duct 1 with height h_1 and duct 2 with height h_2. Non-uniform mean flow is present in duct 1 and is assumed to continue in duct 2 with unaltered profile.

with boxed numbers 1 and 2, respectively. In duct 1 parallel non-uniform mean flow is present. The mean flow is assumed to continue with unaltered profile in duct 2, where thus only partially non-uniform flow is present.

The Euler equations for conservation of momentum and mass equations, describing the motion of a perfect and isentropic fluid:

$$\rho \frac{\mathrm{D}\vec{v}}{\mathrm{D}t} = -\vec{\nabla} p, \tag{1}$$

$$\frac{1}{\rho}\frac{\mathrm{D}\rho}{\mathrm{D}t} = -\vec{\nabla} \cdot \vec{v}, \tag{2}$$

and

$$c^2 \frac{\mathrm{D}\rho}{\mathrm{D}t} = \frac{\mathrm{D}p}{\mathrm{D}t}, \tag{3}$$

with

$$\frac{\mathrm{D}}{\mathrm{D}t} = \frac{\partial}{\partial t} + \vec{v} \cdot \vec{\nabla}$$

with ρ the mass density, p the pressure, $\vec{v}$ the velocity vector and c the speed of sound, are linearized according to: $c = c_0 + c'$, $\rho = \rho_0 + \rho'$, $p = p_0 + p'$, where $\rho' \ll \rho_0$, and $\vec{v} = U(y)\vec{e}_x + u'\vec{e}_x + v'\vec{e}_y$, with $\vec{e}_x$, $\vec{e}_y$ unit vectors in the x- and y-direction, to obtain

$$\rho_0\left(\frac{\partial}{\partial t} + U\frac{\partial}{\partial x}\right)u' + \rho_0 \frac{\mathrm{d}U}{\mathrm{d}y}v' = -\frac{\partial p'}{\partial x}, \tag{4}$$

$$\rho_0\left(\frac{\partial}{\partial t} + U\frac{\partial}{\partial x}\right)v' = -\frac{\partial p'}{\partial y}, \tag{5}$$

$$\frac{1}{\rho_0 c_0^2}\left(\frac{\partial}{\partial t} + U\frac{\partial}{\partial x}\right)p' = -\left(\frac{\partial u'}{\partial x} + \frac{\partial v'}{\partial y}\right). \tag{6}$$

Taking $\rho_0(\partial/\partial t + U(\partial/\partial x))$ (6) and subtracting $\partial/\partial x$ (4) and $\partial/\partial y$ (5) gives

$$\frac{1}{c_0^2}\left(\frac{\partial}{\partial t} + U\frac{\partial}{\partial x}\right)^2 p' - \left(\frac{\partial^2 p'}{\partial x^2} + \frac{\partial^2 p'}{\partial y^2}\right) = 2\rho_0 \frac{\mathrm{d}U}{\mathrm{d}y}\frac{\partial v'}{\partial x}. \tag{7}$$

Subsequently, the following non-dimensionalization of the relevant quantities is employed:

$$\begin{aligned} &p_* = \frac{1}{\rho_0 c_0^2}p', \quad (x_*, y_*, h_{1*}, h_{2*}) = \left(\frac{x}{h_1}, \frac{y}{h_1}, 1, \frac{h_2}{h_1}\right), \\ &(u_*, v_*) = \frac{1}{c_0}(u', v'), \quad \omega_* = \frac{\omega h_1}{c_0}, \\ &M(y) = M_0 f(y) = \frac{1}{c_0}U(y), \quad t_* = \frac{c_0 t}{h_1}, \end{aligned} \tag{8}$$

with M the Mach number and ω the angular frequency of sound. The function $f(y)$ prescribes the profile of the mean flow. M_0 is a fixed number, which is generally chosen to give the y-averaged Mach number in duct 1. Furthermore, harmonic waves in the x-direction are assumed, giving the following complex forms:

$$\begin{aligned} p_* &= P(y_*)\exp(-\mathrm{i}k_* x_*)\exp(\mathrm{i}\omega_* t_*), \\ v_* &= V(y_*)\exp(-\mathrm{i}k_* x_*)\exp(\mathrm{i}\omega_* t_*), \\ q_* &= Q(y_*)\exp(-\mathrm{i}k_* x_*)\exp(\mathrm{i}\omega_* t_*), \end{aligned} \tag{9}$$

with $i^2 = -1$. Here, we have introduced the quantity q_* for later use:

$$q_* = i\frac{\partial p_*}{\partial x_*}. \tag{10}$$

k_* is the dimensionless wavenumber according to: $k_* = kh_1$, where k is the wavenumber with dimension. Finally, the problem is solved by the finite difference method. Therefore, discretization in the y_*-coordinate is employed by taking N_1 equally spaced points in duct 1 and N_2 equally spaced points in duct 2. The spacing between interior points in both ducts 1 and 2 is $\Delta h = h_1/N_1 = h_2/N_2$, or $\Delta h_* = h_{1*}/N_1 = 1/N_1$. The first and last point is taken half a spacing, i.e. $h_{1*}/2N_1 = 1/2N_1$, from the duct wall. Substituting the forms of Eq. (9) in Eqs. (5) and (7), after employing the non-dimensionalization of Eq. (8), gives, with the above-mentioned discretization, the following generalized eigenvalue problem for modes in duct 1:

$$k_*\begin{pmatrix} \mathbf{I} - M_0^2\mathbf{f}^2 & 2iM_0\mathbf{f}_a & \mathbf{0} \\ \mathbf{0} & iM_0\mathbf{f} & \mathbf{0} \\ \mathbf{0} & \mathbf{0} & \mathbf{I} \end{pmatrix}\begin{pmatrix} \mathbf{Q} \\ \mathbf{V} \\ \mathbf{P} \end{pmatrix} = \begin{pmatrix} -2\omega_* M_0\mathbf{f} & \mathbf{0} & \omega_*^2\mathbf{I} + \mathbf{D}_2 \\ \mathbf{0} & i\omega * \mathbf{I} & \mathbf{D}_1 \\ \mathbf{I} & \mathbf{0} & \mathbf{0} \end{pmatrix}\begin{pmatrix} \mathbf{Q} \\ \mathbf{V} \\ \mathbf{P} \end{pmatrix}. \tag{11}$$

Here $\mathbf{I}$ is the $(N_1 \times N_1)$ identity matrix. $\mathbf{P}$ and $\mathbf{V}$ are $(N_1 \times 1)$ column vectors giving the value of $P(y)$ and $V(y)$ at the discrete points. $\mathbf{f}$, $\mathbf{f}^2$ and $\mathbf{f}_a$ are $(N_1 \times N_1)$ matrices with on their diagonal the values of $f(y_*), f^2(y_*)$ and $df(y_*)/dy_*$, respectively, at the discrete points in duct 1. $\mathbf{D}_1$ and $\mathbf{D}_2$ are $(N_1 \times N_1)$ matrices giving the first-, respectively, second-order differential operator with respect to y_*. These matrices also account for the boundary condition $\partial p_*/\partial y_* = 0$ at the duct walls. From the definition of q_*, see Eq. (10), and Eq. (9) it follows that: $Q(y) = k_* P(y)$, or in discrete form: $\mathbf{Q} = k_*\mathbf{P}$. Solving the eigenvalue problem (11) gives all eigenvectors, i.e. modes, $\mathbf{Q}_e$ and $\mathbf{P}_e$ and $\mathbf{V}_e$, as well as the corresponding eigenvalues, i.e. dimensionless wavenumbers, k_{e*}, in duct 1. In total $3N_1$ modes are found, which can generally be divided in N_1 acoustic modes propagating (or decaying) in the $+x$-direction, N_1 acoustic modes propagating (or decaying) in the $-x$-direction, and N_1 hydrodynamic modes propagating in the direction of the mean flow ($+x$-direction). The total solution for q_*, and the non-dimensional pressure and velocity disturbance p_*, respectively, v_* at the discrete points is a linear combination of these modes:

$$\begin{aligned} \mathbf{q}_*(x_*, t_*) &= \sum_{n=1}^{3N_1} C_n \mathbf{Q}_{e,n} \exp(-ik_{e,n*}x_*)\exp(i\omega_* t_*), \\ \mathbf{v}_*(x_*, t_*) &= \sum_{n=1}^{3N_1} C_n \mathbf{V}_{e,n} \exp(-ik_{e,n*}x_*)\exp(i\omega_* t_*), \\ \mathbf{p}_*(x_*, t_*) &= \sum_{n=1}^{3N_1} C_n \mathbf{P}_{e,n} \exp(-ik_{e,n*}x_*)\exp(i\omega_* t_*) \end{aligned} \tag{12}$$

with n an index for the modes and C_n the coefficient of mode n. Note here that if the eigenvalue problem has a certain solution k_*, $\mathbf{Q}$, $\mathbf{V}$, $\mathbf{P}$, also k_*^*, $\mathbf{Q}^*$, $-\mathbf{V}^*$, $\mathbf{P}^*$ is a solution, where superscript $*$ denotes the complex conjugate. Solutions are thus found in complex conjugate pairs.

For duct 2 an analogous generalized eigenvalue problem as Eq. (11) can be derived for the eigenmodes and accompanying wavenumbers. However, in duct 2 non-uniform mean flow is only present at the first N_1 points, for $y < h_1$. The fact that the mean flow velocity and its derivative are zero for the $N_2 - N_1$ discrete points at $y > h_1$ has the consequence that an equal number of rows and columns in the matrix in the left-hand side of the generalized eigenvalue problem, Eq. (11), become zero. The concerning rows correspond to the equations for the elements of vector $\mathbf{V}$ at these discrete points where mean flow is absent. The 'zero-columns' correspond to the same elements of $\mathbf{V}$ as they are used as input for the other equations on the rows of Eq. (11). Clearly, for the generalized eigenvalue problem to remain solvable in duct 2, these 'zero-rows and -columns', as well as the corresponding ones in the matrix in the right-hand side of Eq. (11), have to be omitted. This means that in the generalized eigenvalue problem for duct 2 $\mathbf{V}$ is only defined for the (first) N_1 points, at which mean flow is present. Note that in principle the values of V at the discrete points where mean flow is absent can be deduced from the pressure modes. The total number of equations and the total number of unknowns ($\mathbf{Q}$, $\mathbf{V}$ and $\mathbf{P}$) in

duct 2 is thus $2N_2 + N_1$. Generally, in duct 2 a number of N_2 acoustic modes propagating (or decaying) in the $+x$-direction and N_2 acoustic modes propagating (or decaying) in the $-x$-direction are obtained. Since hydrodynamic modes are associated with sheared mean flow, a number N_1 of them, equal to the number of discrete point with flow, are found.

2.2. Uniform flow

In case uniform mean flow, instead of non-uniform mean flow, is assumed in duct 1, it can be shown that the vector $\mathbf{V}$ is not needed anymore in Eq. (11), in order to solve the modes. Consequently, in formulating an eigenvalue problem for duct 1 with uniform flow, the use of vectors $\mathbf{Q}$ and $\mathbf{P}$ is sufficient, and the vector $\mathbf{V}$ can be omitted:

$$k_* \begin{pmatrix} (1-M_0^2)\mathbf{I} & \mathbf{0} \\ \mathbf{0} & \mathbf{I} \end{pmatrix} \begin{pmatrix} \mathbf{Q} \\ \mathbf{P} \end{pmatrix} = \begin{pmatrix} -2\omega_* M_0 \mathbf{I} & \omega_*^2 \mathbf{I} + \mathbf{D}_2 \\ \mathbf{I} & \mathbf{0} \end{pmatrix} \begin{pmatrix} \mathbf{Q} \\ \mathbf{P} \end{pmatrix}. \tag{13}$$

Here, M_0 is the uniform mean flow Mach number. Note that when mean flow is completely absent in the duct, the same formulation of the eigenvalue problem as above can be used with $M_0 = 0$ substituted. Solving Eq. (13) with N_1 discrete points in duct 1 generally gives N_1 acoustic modes propagating/decaying in the $+x$-direction, and N_1 acoustic modes propagating/decaying in the $-x$-direction. No hydrodynamic modes are found, since the mean flow is not sheared.

In duct 2 uniform mean flow is present only for $y < h_1$, whereas for $y > h_1$ the fluid is quiescent. The mean flow is thus discontinuous in y, and an infinitely thin shear layer is present at $y = h_1$. Here, special care has to be taken to ensure that the pressure disturbance and the fluid displacement in transverse direction are continuous over the shear layer. For this purpose an additional point is introduced in duct 2 halfway between point N_1 and $N_1 + 1$, at the position of the infinitely thin shear layer. At this point we consider the amplitude P_{flow}, respectively, V_{flow} of the acoustic pressure and velocity in y-direction as 'seen' from the region with flow, as well as the acoustic pressure and velocity amplitude, P_{noflow}, respectively, V_{noflow}, seen from the no flow region. Employing a second-order expansion in Δh_* for $P(y_*)$ around $y_* = 1$ it can be deduced that

$$\begin{aligned} P_{\text{flow}} &= \frac{-\mathbf{P}(N_1-1) + 9\mathbf{P}(N_1)}{8} - \frac{3\mathrm{i}\Delta h_*(\omega_* - M_0 k_*)V_{\text{flow}}}{8}, \\ P_{\text{noflow}} &= \frac{9\mathbf{P}(N_1+1) - \mathbf{P}(N_1+2)}{8} + \frac{3\mathrm{i}\Delta h_* \omega_* V_{\text{noflow}}}{8}. \end{aligned} \tag{14}$$

Furthermore, the second derivative accurate to order $(\Delta h_*)^2$ of the acoustic pressure amplitude at points N_1 and $N_1 + 1$ changes into:

$$\begin{aligned} \left.\frac{\mathrm{d}^2 P}{\mathrm{d}y_*^2}\right|_{N_1} &= \frac{\mathbf{P}(N_1-1) - \mathbf{P}(N_1)}{(\Delta h_*)^2} - \frac{\mathrm{i}(\omega_* - M_0 k_*)V_{\text{flow}}}{\Delta h_*}, \\ \left.\frac{\mathrm{d}^2 P}{\mathrm{d}y_*^2}\right|_{N_1+1} &= \frac{-\mathbf{P}(N_1+1) + \mathbf{P}(N_1+2)}{(\Delta h_*)^2} + \frac{\mathrm{i}\omega_* V_{\text{noflow}}}{\Delta h_*} \end{aligned} \tag{15}$$

given that these points are interior points, i.e. the boundary condition for the pressure at the duct walls is not 'felt' at these points. Demanding continuity of pressure at the interface between mean flow and no mean flow yields: $P_{\text{flow}} = P_{\text{noflow}}$, and hence from Eq. (14):

$$\begin{aligned} 3\mathrm{i}\Delta h_* M_0 k_* V_{\text{flow}} = {} & \mathbf{P}(N_1-1) - 9\mathbf{P}(N_1) + 9\mathbf{P}(N_1+1) - \mathbf{P}(N_1+2) \\ & + 3\mathrm{i}\Delta h_* \omega_* V_{\text{flow}} + 3\mathrm{i}\Delta h_* \omega_* V_{\text{noflow}}. \end{aligned} \tag{16}$$

Furthermore, the transverse acoustic fluid displacement in complex non-dimensional form:

$$\delta_* = D(y_*)\exp(-\mathrm{i}k_* x_*)\exp(\mathrm{i}\omega_* t_*), \tag{17}$$

is given by the convective derivative of the transverse velocity

$$\mathrm{i}(\omega_* - M_0 f k_*)D = V. \tag{18}$$

The additional continuity of displacement required at the interface, i.e. the vortex sheet thus gives

$$M_0 k_* V_{\text{noflow}} = \omega_* V_{\text{noflow}} - \omega_* V_{\text{flow}}. \tag{19}$$

Eqs. (16) and (19) can now be incorporated in order to get the eigenvalue problem for duct 2 with the infinitely thin shear layer:

$$k_* \begin{pmatrix} \mathbf{I} - M_0^2\mathbf{f}^2 & \mathbf{0} & \mathbf{0} & \mathbf{0} \\ \mathbf{0} & \mathbf{I} & \mathbf{0} & \mathbf{0} \\ \mathbf{0} & \mathbf{0} & 3\mathrm{i}\Delta h_* M_0 & 0 \\ \mathbf{0} & \mathbf{0} & 0 & M_0 \end{pmatrix} \begin{pmatrix} \mathbf{Q} \\ \mathbf{P} \\ V_{\text{flow}} \\ V_{\text{noflow}} \end{pmatrix}$$
$$= \begin{pmatrix} -2\omega_* M_0\mathbf{f} & \omega_*^2\mathbf{I} + \mathbf{D}_2 & \mathbf{0} & \mathbf{0} \\ \mathbf{I} & \mathbf{0} & \mathbf{0} & \mathbf{0} \\ \mathbf{0} & \ldots 1, -9, 9, -1 \ldots & 3\mathrm{i}\Delta h_*\omega_* & 3\mathrm{i}\Delta h_*\omega_* \\ \mathbf{0} & \mathbf{0} & -\omega_* & \omega_* \end{pmatrix} \begin{pmatrix} \mathbf{Q} \\ \mathbf{P} \\ V_{\text{flow}} \\ V_{\text{noflow}} \end{pmatrix}, \tag{20}$$

where rows N_1 and N_1+1 of the second-derivative matrix $\mathbf{D}_2$, have to be modified according to Eq. (15). Since this equation is derived for accuracy of order $(\Delta h_*)^2$, only $\mathbf{D}_2$ accurate to order $(\Delta h_*)^2$ can be used. Furthermore, the profile function f here obviously equals 1 for $y<h_1$ (first N_1 points), and 0 for $y>h_1$.

Solving the eigenvalue problem (20) in duct 2 returns the eigenmodes for vectors Q and P as well as the value of V_{flow} and V_{noflow} for the modes. Here, N_2 acoustic modes propagating (or decaying) in the $+x$-direction and N_2 acoustic modes propagating (or decaying) in the $-x$-direction are obtained. Furthermore two hydrodynamic modes are found. These two modes are related to the hydrodynamic instability of the infinitely thin shear layer, known as the Kelvin–Helmholtz instability waves.

2.3. Mode matching

At the interface between the two ducts at $x=0$, cf. Fig. 1, continuity of mass- and momentum flux applies. It can be shown that this yields continuity of the dimensionless pressure and velocity disturbances p_* and v_* as well as continuity of the parameter q_*, where $q_* = \mathrm{i}\partial p_*/\partial x_*$, cf. Eq. (10). In duct 2 the hard wall at $x=0$ for $y>h_1$ yields the condition that the velocity disturbance in the x-direction, normal to the wall, is zero. This implies that $q_*=0$ for $y>h_1$. For the case of non-uniform flow the above-stated conditions at $x=0$ applied at the discrete points yield, with the modal expansion for the discretized parameters $\mathbf{q}_*$, $\mathbf{v}_*$ and $\mathbf{p}_*$, given by Eq. (12), the following system of $2N_1+N_2$ equations:

$$\underbrace{\begin{pmatrix} -\mathbf{Q}_1^- & \mathbf{Q}_2^+ \\ \mathbf{0} & \\ -\mathbf{V}_1^- & \mathbf{V}_2^+ \\ -\mathbf{P}_1^- & \mathbf{P}_2^+(1:N_1,:) \end{pmatrix}}_{\mathbf{S}_1} \begin{pmatrix} \mathbf{C}_1^- \\ \mathbf{C}_2^+ \end{pmatrix} = \underbrace{\begin{pmatrix} \mathbf{Q}_1^+ & -\mathbf{Q}_2^- \\ \mathbf{0} & \\ \mathbf{V}_1^+ & -\mathbf{V}_2^- \\ \mathbf{P}_1^+ & -\mathbf{P}_2^-(1:N_1,:) \end{pmatrix}}_{\mathbf{S}_2} \begin{pmatrix} \mathbf{C}_1^+ \\ \mathbf{C}_2^- \end{pmatrix}. \tag{21}$$

Here, the eigenmodes $\mathbf{Q}_e$, $\mathbf{V}_e$ and $\mathbf{P}_e$ are the columns of matrices $\mathbf{Q}$, $\mathbf{V}$ and $\mathbf{P}$. The additional subscripts 1 and 2 refer to duct 1 and 2, respectively. The use of superscripts $+$ and $-$ reflects a distinction between modes propagating to the $+x$-direction (acoustic and hydrodynamic) and the $-x$-direction (only acoustic). Vectors $\mathbf{C}$ contain the coefficients of the modes. The continuity of pressure only applies for $y\leqslant h_1$, thus at the first N_1 discrete points. Therefore, only the first N_1 rows of $\mathbf{P}_2^+$ and $\mathbf{P}_2^-$, containing the pressure disturbance modes, are considered in the equation above. This is indicated by the additional $(1:N_1,:)$ behind matrices $P_2^{\pm}$. Both matrices $\mathbf{S}_1$ and $\mathbf{S}_2$ in Eq. (21) are square with size $(2N_1+N_2)\times(2N_1+N_2)$. $\mathbf{S}_1$ can be inverted to obtain the scattering matrix: $\mathbf{S}=\mathbf{S}_1^{-1}\mathbf{S}_2$. This matrix relates the coefficients of all modes propagating away from the area

expansion in the duct to the coefficients of the modes propagating towards the area expansion:

$$\begin{pmatrix} \mathbf{C}_1^- \\ \mathbf{C}_2^+ \end{pmatrix} = \mathbf{S} \begin{pmatrix} \mathbf{C}_1^+ \\ \mathbf{C}_2^- \end{pmatrix}. \tag{22}$$

The scattering matrix contains the complete aero-acoustical behaviour of the area expansion geometry.

In many cases, and also in this paper, only frequencies which are low enough, such that only the (quasi-) plane waves are propagating (cut-on), are considered. Acoustic energy is then solely carried by these plane waves, and only their scattering at the area expansion is of interest. Reflection and transmission coefficients of the plane wave pressure disturbance at the duct expansion can be defined in either direction. When sorting the above given eigenmode matrices $\mathbf{Q}$, $\mathbf{V}$, $\mathbf{P}$ such that the plane wave modes, both for $+x$ and $-x$ propagating, are in the first column, they are given by

$$\begin{aligned} R^+ &= \frac{\mathbf{C}_1^-(1)}{\mathbf{C}_1^+(1)} = \mathbf{S}(1,1), \quad T^- = \frac{\mathbf{C}_1^-(1)}{\mathbf{C}_2^{-(1)}} = \mathbf{S}(1, 2N_1+1), \\ T^+ &= \frac{\mathbf{C}_2^+(1)}{\mathbf{C}_1^{+(1)}} = \mathbf{S}(N_1+1, 1), \quad R^- = \frac{\mathbf{C}_2^+(1)}{\mathbf{C}_2^-(1)} = \mathbf{S}(N_1+1, 2N_1+1). \end{aligned} \tag{23}$$

It has to be noted here that all calculated plane wave modes have to be equally normalized first for these relations to be useful. Therefore, in calculations the y-averaged amplitude of the pressure disturbance plane wave modes are set to unity.

In the same way a mode-matching procedure can be done for the case of uniform flow (infinitely thin shear layer). Here, in duct 2 the velocity disturbance in the y-direction at the side with mean flow and the side without mean flow is available as an extra parameter at the position of the shear layer. The amplitude of these variables were denoted V_{flow} and V_{noflow}, respectively. The latter will now be used to apply a Kutta condition at the edge of the area discontinuity at $x = 0, y = h_1$. The Kutta condition states that the flow leaves the edge tangentially, such that the fluid displacement δ as well as the derivative of the displacement with respect to x equals zero at the edge:

$$\delta = 0, \quad \frac{\partial \delta}{\partial x} = 0 \quad \text{at } x = 0, \quad y = h_1. \tag{24}$$

The velocity disturbance equals the convective derivative of the displacement, Eq. (18), such that from Eq. (24) the condition: $V_{\text{noflow}} = 0, k_* V_{\text{noflow}} = 0$ is obtained at $x = 0$. Note that for simplicity this is in a 'single mode' notation. In effect these conditions apply for the sum over all the modes. Incorporating the Kutta condition in the matching of pressure and mass flux between duct 1 and 2 gives for uniform flow, analogous to Eq. (21):

$$\underbrace{\begin{pmatrix} -\mathbf{Q}_1^- & \mathbf{Q}_2^+ \\ \mathbf{0} & \\ -\mathbf{P}_1^- & \mathbf{P}_2^+(1:N_1,:) \\ \mathbf{0} & \mathbf{V}_{\text{nf}}^+ \\ \mathbf{0} & \mathbf{V}_{\text{nf}}^+ \mathbf{k}_2^+ \end{pmatrix}}_{\mathbf{S}_1} \begin{pmatrix} \mathbf{C}_1^- \\ \mathbf{C}_2^+ \end{pmatrix} = \underbrace{\begin{pmatrix} \mathbf{Q}_1^+ & -\mathbf{Q}_2^- \\ \mathbf{0} & \\ \mathbf{P}_1^+ & -\mathbf{P}_2^-(1:N_1,:) \\ \mathbf{0} & -\mathbf{V}_{\text{nf}}^- \\ \mathbf{0} & -\mathbf{V}_{\text{nf}}^- \mathbf{k}_2^- \end{pmatrix}}_{\mathbf{S}_2} \begin{pmatrix} \mathbf{C}_1^+ \\ \mathbf{C}_2^- \end{pmatrix}. \tag{25}$$

Here, the value of V_{noflow} for the modes are in the (single value) columns of matrix $\mathbf{V}_{\text{nf}}$. As for the other matrices containing modes for pressure disturbance etc. a distinction between $+x$-propagating and $-x$-propagating modes is made denoted by the additional superscripts. Matrices $\mathbf{k}_2$ contain the values of the wavenumbers in duct 2 on the diagonal, such that $\mathbf{V}_{\text{nf}}\mathbf{k}_2$ gives the modes multiplied by their corresponding wavenumber. In the equation above $\mathbf{S}_1$ measures $(N_1+N_2+2) \times (N_1+N_2+2)$ and $\mathbf{S}_2$ measures $(N_1+N_2+2) \times (N_1+N_2)$. Since $\mathbf{S}_1$ is square it can (in general) be inverted. Subsequent multiplication with $\mathbf{S}_2$ gives the $(N_1+N_2+2) \times (N_1+N_2)$ scattering matrix $\mathbf{S}$ analogous to Eq. (22). The reflection and

transmission coefficients of the plane waves are now given by

$$R^+ = \mathbf{S}(1,1), \quad T^- = \mathbf{S}(1, N_1+1),$$
$$T^+ = \mathbf{S}(N_1+1, 1), \quad R^- = \mathbf{S}(N_1+1, N_1+1). \tag{26}$$

Both the procedure to solve the modes and wavenumbers and the mode-matching are implemented in Matlab. In the preceding already a distinction between acoustic modes propagating/decaying either to the right ($+x$-direction) or the left ($-x$-direction) and hydrodynamic modes propagating with the mean flow to the right is discussed. Formally, when the modes are solved their direction of propagation is unknown. In order to determine the direction of propagation two causality criteria can be used: the Briggs–Bers formalism [34,35] and the Crighton–Leppington [36] formalism. Note, however, that the Briggs–Bers formalism is not applicable in the case of an infinitely thin shear layer [37]. Once the direction of the propagation of all modes is known the mode-matching can be performed. A further identification of the modes can be done on basis of their wavenumbers and phase velocities. In any case the plane waves need to be identified in order to calculate their scattering coefficient. Here in most cases a full identification of all modes could be made in first instance on basis of their wavenumber (and phase velocity). In some cases a distinction between the hydrodynamic unstable modes and the first higher-order evanescent acoustic modes could not readily be made on basis of the value of the wavenumber. Both causality criteria were then used to solve this.

2.4. 2D cylindrical geometry

The multimodal method to obtain the sound scattering at a sudden area expansion in a 2D rectangular duct has been derived above. The method can analogously be derived for 2D cylindrical geometry. In that case the y-dependency of variables is replaced by a dependency on the radial coordinate r, and the duct heights h_1 and h_2 become duct radii r_1 and r_2, with non-dimensionalization $r_* = r/r_1$. Furthermore, the difference between divergence in a Cartesian coordinate system and in a cylindrical coordinate system has to be taken into account in Eqs. (1) and (2). It can be shown then that exactly the same eigenvalue problems for the modes and wavenumbers are obtained as given by Eqs. (11), (13), and (20). Only the term $\omega^2\mathbf{I} + \mathbf{D}_2$ in the right-hand side matrix is replaced by $\omega^2\mathbf{I} + \mathbf{D}_2 + \mathbf{r}_*^{-1}\mathbf{D}_1$. Here, matrix $\mathbf{r}_*^{-1}\mathbf{D}_1$ represents the discretization of $(1/r_*)(\mathrm{d}P/\mathrm{d}r_*)$. The mode-matching procedures are the same as in 2D rectangular geometry.

3. Results

3.1. Infinitely thin shear layer: comparison with alternative models

First, results for the scattering of plane waves at a sudden area expansion in a duct with uniform flow, yielding an infinitely thin shear layer, as obtained by the multimodal method are compared to results from the model by Boij and Nilsson [12,28]. The model they presented was for a 2D rectangular duct geometry. However, they proposed a scaling between 2D rectangular and 2D cylindrical geometry, such that comparison with experimental data of Ronneberger [1,4], obtained for an expansion in a cylindrical duct, could be made. Here, multimodal analysis calculations for an area expansion in 2D rectangular are compared to Boij and Nilsson's model results. Also calculations for 2D cylindrical geometry are presented and compared to the 2D rectangular calculations in order to test the scaling rule.

Boij and Nilsson [12] reasoned that for low frequencies well below the cut-on of the first higher-order acoustic mode, only a plane wave is incident on the area expansion. For cylindrical geometry the incident sound pressure field is then independent of the angular coordinate, and consequently higher-order modes which are only dependent on the radial coordinate (radial modes) will be excited at the expansion. From this they assumed that the area expansion in a cylindrical duct can be considered to be a 2D problem, and hence can be related to their theory for a 2D rectangular duct. Furthermore, they argued that the predominant feature is the onset of higher-order modes in the large duct downstream of the expansion. For low frequency the wavelength is much larger than the transverse dimension of the duct, such that geometrical details will not be resolved by the sound field. The plane wave scattering at the area expansion would therefore be reasonably

similar for a rectangular and a cylindrical duct if the area expansion ratio is the same, and provided that the frequency is normalised by the cut-on frequency of the first higher-order mode in the downstream duct. This leads to their definition of the normalized Helmholtz number:

$$He^* = \frac{(k_0 h_2)_{\text{rec}}}{(k_0 h_2)_0} = \frac{(k_0 r_2)_{\text{cyl}}}{(k_0 r_2)_0}. \tag{27}$$

Here $(k_0 h_2)_{\text{rec}}$ and $(k_0 r_2)_{\text{cyl}}$ are the Helmholtz numbers based on the downstream duct height h_2 and the downstream duct radius r_2 in rectangular and cylindrical geometry, respectively. $(k_0 h_2)_0$ and $(k_0 r_2)_0$ are the cut-on Helmholtz numbers for the first higher-order mode (without mean flow) for the downstream rectangular and cylindrical duct, respectively. They are given by $(k_0 h_2)_0 = \pi$ and $(k_0 r_2)_0 = \kappa_0 \approx 3.832$. The area expansion ratio η is given by

$$\eta = \frac{h_1}{h_2} = \frac{r_1^2}{r_2^2} \tag{28}$$

with h_1 and r_1 the height, respectively, radius of the smaller upstream duct. Combining Eqs. (27), (28) above gives

$$He^* = \frac{1}{\eta}\frac{(k_0 h_1)_{\text{rec}}}{\pi} = \frac{1}{\sqrt{\eta}}\frac{(k_0 r_1)_{\text{cyl}}}{\kappa_0}, \tag{29}$$

with $(k_0 h_1)_{\text{rec}}$ and $(k_0 r_1)_{\text{cyl}}$ the Helmholtz numbers based on the upstream duct height, respectively, the upstream duct radius in rectangular and cylindrical geometry.

Figs. 2–4 show the magnitude, respectively, phase of the upstream reflection coefficient R^+ for plane waves, respectively, the magnitude of the downstream transmission coefficient T^+ for plane waves at an area expansion in a 2D rectangular duct as obtained by the current multimodal method and as presented by Boij and Nilsson [12,28]. The Helmholtz number on the upstream duct is $k_0 h_1 = 0.11$, and the area expansion ratio is $\eta = h_1/h_2 = 0.35$. The number of discrete points used in the multimodal method is $N_1 = 70$ in the upstream duct and $N_2 = 200$ in the downstream duct. At these values the results were found to be converged, i.e. increasing the number of points gave no significant difference in the results for the scattering coefficients.

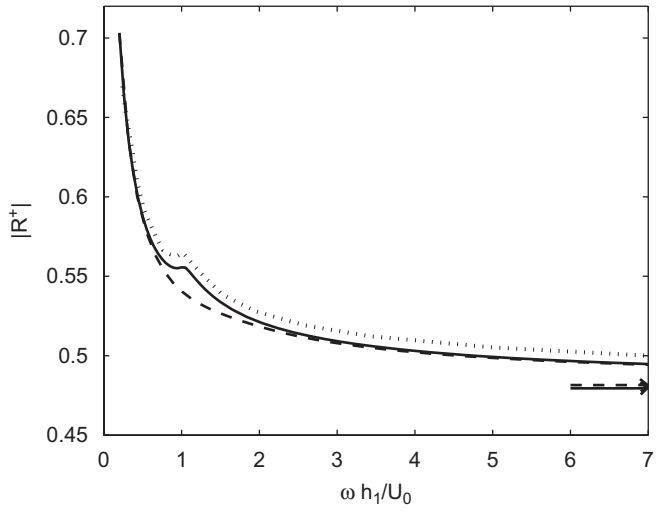

Fig. 2. Magnitude of the downstream reflection coefficient R^+ at an area expansion in a duct with uniform flow versus Strouhal number $\omega h_1/U_0$ (by varying the Mach number). Calculations for a 2D rectangular geometry with Helmholtz number on upstream duct height $k_0 h_1 = 0.11$ and area expansion ratio of $\eta = h_1/h_2 = 0.35$. Solid line: multimodal method with number of points $N_1 = 70$, $N_2 = 200$. Dotted line: fit of Boij and Nilsson's result [12,28]. Also the quasi-steady limit without flow and the result of multimodal analysis without flow are indicated by the dashed and solid arrows, respectively. The dashed line gives the multimodal analysis result for a 2D cylindrical geometry with the same area expansion ratio and normalized Helmholtz number, $He^* = 0.10$, yielding $k_0 r_1 = 0.2268$. Here $N_1 = 100$ and $N_2 = 169$.

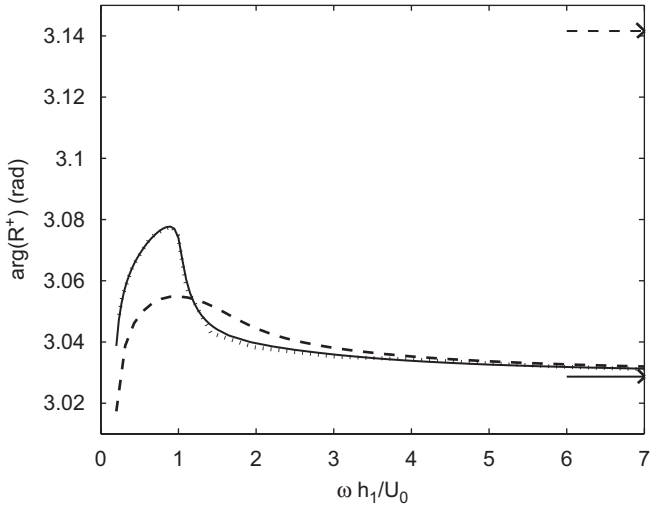

Fig. 3. Phase of the downstream reflection coefficient R^+ at an area expansion in a duct with uniform flow versus Strouhal number $\omega h_1/U_0$ (by varying the Mach number). Calculations for a 2D rectangular geometry with Helmholtz number on upstream duct height $k_0h_1 = 0.11$ and area expansion ratio of $\eta = h_1/h_2 = 0.35$. Data indication as in Fig. 2.

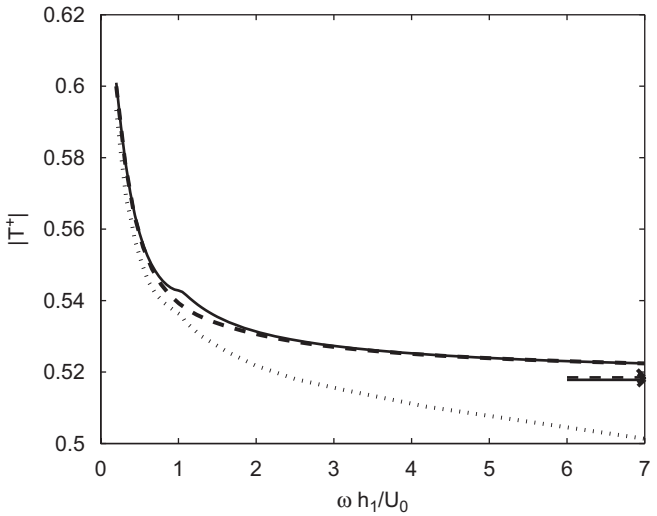

Fig. 4. Magnitude of the downstream transmission coefficient T^+ at an area expansion in a duct with uniform flow versus Strouhal number $\omega h_1/U_0$ (by varying the Mach number). Calculations for a 2D rectangular geometry with Helmholtz number on upstream duct height $k_0h_1 = 0.11$ and area expansion ratio of $\eta = h_1/h_2 = 0.35$. Data indication as in Fig. 2.

Results are calculated for various Mach numbers $M_0 = U_0/c_0$, and are plotted versus Strouhal number $\omega h_1/U_0$ in the figures. Also the quasi-steady limit as well as the results obtained by multimodal analysis in absence of mean flow are indicated by the dashed and solid arrows, respectively. The results of the multimodal method and the model of Boij and Nilsson are very similar. In particular, both show the hump in reflection and transmission around Strouhal number 1. For the phase of R^+ no significant difference is seen between the two models (the difference seen in the graph is in the order of the inaccuracy in extracting the data from Ref. [12]). Nevertheless, a deviation in the results for the absolute values is seen. Generally, the mode-matching method gives a lower absolute value for the reflection coefficient and a higher one for the transmission coefficient than Boij and Nilsson's model. For the absolute value of the reflection coefficient the deviation

between the two models is fairly constant at about 1%, at least above a Strouhal number of ~0.5. The absolute value of the transmission coefficient displays a larger deviation, it increases from about 1% for low Strouhal number to about 4% for high Strouhal number. In particular the result for the absolute value of the transmission coefficient obtained by Boij and Nilsson does not seem to approach the quasi-steady result (or multimodal result without flow, which accounts for the finite frequency) for high Strouhal number, i.e. low flow velocity, whereas the result obtained by the multimodal method does.

Furthermore Figs. 2–4 also show the results obtained by the multimodal method for the equivalent 2D cylindrical geometry. According to the scaling proposed by Boij and Nilsson, discussed above, here the expansion ratio is the same: $\eta = r_1^2/r_2^2 = 0.35$, and the Helmholtz number on the upstream duct radius is $k_0 r_1 = 0.227$, giving a normalized Helmholtz number of $He^* = 0.10$ for both rectangular and cylindrical geometry, cf. Eq. (29). For the cylindrical geometry the number of discrete points was $N_1 = 100$ and $N_2 = 169$ in duct 1 and 2, respectively. The values for the reflection and transmission coefficients are calculated at the same Mach numbers as in the 2D rectangular case, and similarly plotted versus $\omega h_1/U_0$. Generally, the absolute values of the two displayed scattering coefficients are reasonably close for the rectangular and equivalent cylindrical calculations. However, around $\omega h_1/U_0 = 1$, corresponding with a Mach number $M_0 = 0.1$, a significant deviation is observed. Here, a hump in the absolute value of the reflection and transmission coefficient is present for the 2D rectangular geometry, whereas this hump is absent for the equivalent 2D cylindrical geometry. It was found that the observed hump is closely related to a particular behaviour of the unstable hydrodynamic modes and the first higher-order evanescent acoustic modes [32]. This behaviour appeared to occur only for duct height ratios, or duct radii ratios of $h_1/h_2 \leqslant 0.5$, respectively, $r_1/r_2 \leqslant 0.5$. In the present case indeed $h_1/h_2 = 0.35 < 0.5$, whereas $r_1/r_2 = 0.59 > 0.5$. Furthermore, Fig. 3 shows a significant difference in the phase of the upstream reflection coefficient below $\omega h_1/U_0 \simeq 4$ when calculated in 2D rectangular or the equivalent 2D cylindrical geometry.

Results for the scattering of plane waves at an area expansion in a 2D cylindrical duct with uniform mean flow obtained by the current multimodal method are also compared to results obtained by the simplified multimodal method of Aurégan [22,23] described in the introduction. For the configuration $k_0 r_1 = 0.227$, $\eta = r_1^2/r_2^2 = 0.35$ the calculated magnitude and phase of the upstream reflection coefficient R^+ and the downstream transmission coefficient T^+ are plotted as function of the Mach number in Figs. 5 and 6,

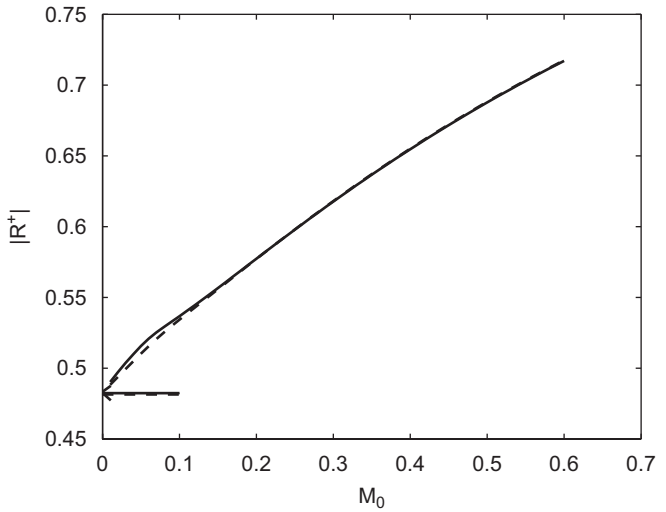

Fig. 5. Magnitude of the downstream reflection coefficient R^+ at an area expansion in a 2D cylindrical duct with uniform flow versus Mach number M_0. Helmholtz number on upstream duct radius is $k_0 h_1 = 0.227$ and area expansion ratio is $\eta = r_1^2/r_2^2 = 0.35$. Solid line: result of current multimodal method, $N_1 = 100$, $N_2 = 169$. Dashed line: result of simplified multimodal method by Aurégan [22,23]. Also the quasi-steady limit and the result obtained with the current multimodal method in absence of mean flow are indicated by the dashed and solid arrow, respectively.

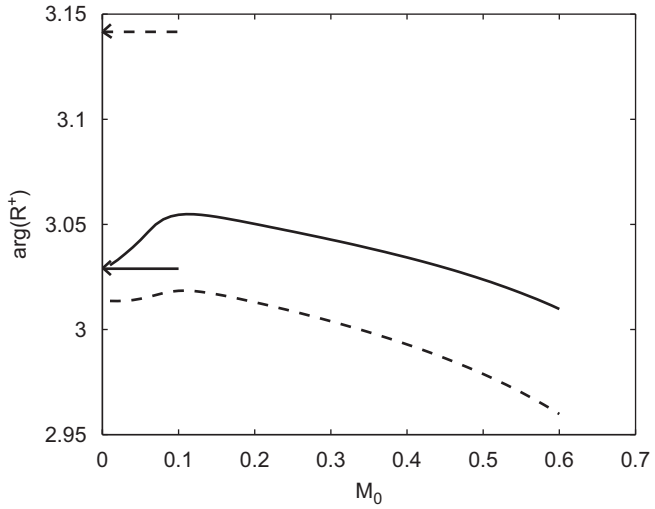

Fig. 6. Phase of the downstream reflection coefficient R^+ at an area expansion in a 2D cylindrical duct with uniform flow versus Mach number M_0. Helmholtz number on upstream duct radius is $k_0h_1 = 0.227$ and area expansion ratio is $\eta = r_1^2/r_2^2 = 0.35$. Data indication as in Fig. 5.

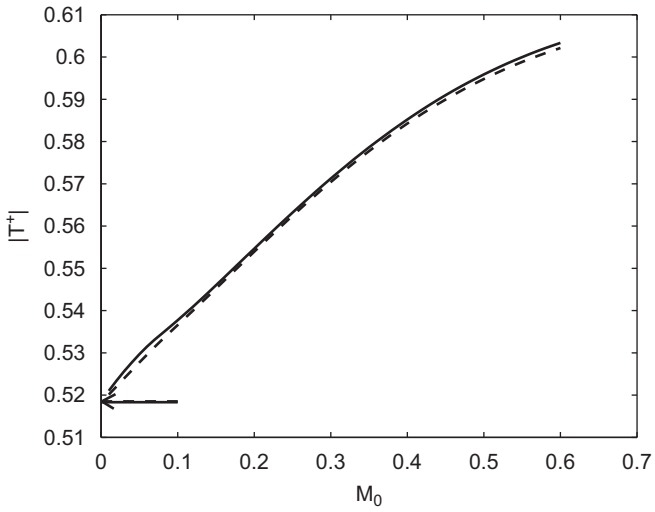

Fig. 7. Magnitude of the downstream transmission coefficient T^+ at an area expansion in a 2D cylindrical duct with uniform flow versus Mach number M_0. Helmholtz number on upstream duct radius is $k_0h_1 = 0.227$ and area expansion ratio is $\eta = r_1^2/r_2^2 = 0.35$. Data indication as in Fig. 5.

respectively, Figs. 7 and 8. The number of discrete points used in the current multimodal method is $N_1 = 100$ and $N_2 = 169$ in ducts 1 and 2, respectively. The result obtained by the two models are quite similar. The difference in the magnitude of the downstream reflection coefficient calculated by the two models is only significant for Mach number less than $\sim$0.15, and is about 0.5% at maximum. The difference found in the phase of the downstream reflection coefficient is reasonably constant at about 0.04 rad ($\sim 0.01\pi$ rad) above a Mach number of 0.1. Below that the difference is less. The deviation between the two models in the magnitude of the downstream transmission coefficient is significant at all Mach numbers (compared to what was seen for the reflection coefficient), but is only about 0.5% at maximum (at $M_0 \simeq 0.05$). The difference in the phase of the downstream transmission coefficient varies with Mach number, and is at maximum about 0.008 rad (0.0025π rad) at $M_0 \simeq 0.01$.

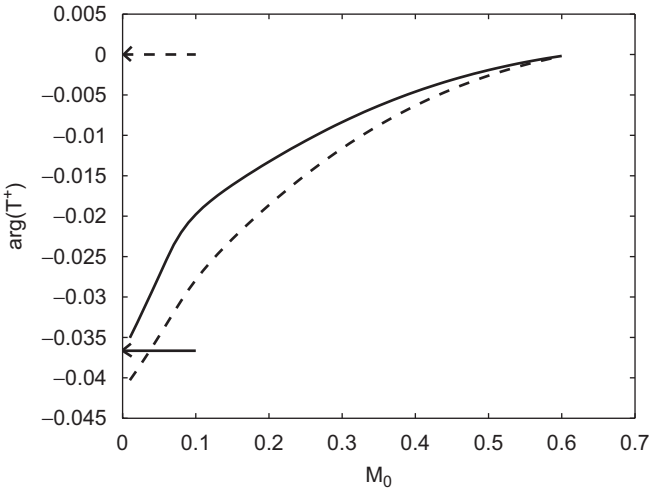

Fig. 8. Phase of the downstream transmission coefficient T^+ at an area expansion in a 2D cylindrical duct with uniform flow versus Mach number M_0. Helmholtz number on upstream duct radius is $k_0h_1 = 0.227$ and area expansion ratio is $\eta = r_1^2/r_2^2 = 0.35$. Data indication as in Fig. 5.

3.2. Comparison with experimental data

Results obtained by the current multimodal method are compared with experimental data of Ronneberger [1,4] for a cylindrical pipe. In the experiments of Ronneberger the pipe radius upstream of the expansion is $r_1 = 25\,\text{mm}$, the pipe radius downstream of the expansion is $r_2 = 42.5\,\text{mm}$. This yields an area expansion ratio of $\eta = 0.35$. Measurements are done at various frequencies and Mach numbers. Here, we will compare with the experiments for which the frequency is $f = 500\,\text{Hz}$. This gives a Helmholtz number on the upstream duct radius of $k_0r_1 = 0.227$. For this configuration scattering results were already presented above for the case of an infinitely thin shear layer. Here, in comparing model results with experimental data, particularly the effect of introducing a non-uniform mean flow, and thus a shear layer with finite thickness, will be investigated.

The flow profile in the upstream tube in Ronneberger's experiments was not measured. However, it can be assumed to obey the empirical power law for turbulent pipe flow as given by Schlichting [38], such that we have

$$f(r) = \begin{cases} \dfrac{(2m+1)(m+1)}{2m^2}\left(1-\dfrac{r}{r_1}\right)^{1/m}, & 0 \leqslant r \leqslant r_1, \\ 0, & r_1 < r \leqslant r_2. \end{cases} \tag{30}$$

The value of the profile function $f(r)$ averaged over the upstream pipe area πr_1^2 equals unity. The Mach number as function of radius is given by: $M(r) = M_0 f(r)$, such that M_0 is the area averaged Mach number in the upstream pipe. The profile parameter m varies with Reynolds number Re on the pipe diameter and the average mean flow velocity:

$$Re = \frac{2r_1U_0}{\nu}, \tag{31}$$

with $U_0 = M_0c_0$ and ν the kinematic viscosity. For air at room temperature (293 K) and atmospheric pressure $\nu = 1.5 \times 10^{-5}\,\text{m}^2\,\text{s}^{-1}$. Values for m at different Reynolds numbers are given in Schlichting [38]. For the measurements with mean flow the Mach numbers are in the range of $M_0 \approx 0.018$ to 0.45. The upstream pipe radius is $r_1 = 2.5 \times 10^{-2}\,\text{m}$. This gives values for the Reynolds number in the range $Re \approx 2.1 \times 10^4$ to $Re \approx 5.1 \times 10^5$. According to Ref. [38] the profile parameter will consequently be between $m \approx 6.5$ for low Mach number and $m \approx 7.7$ for high Mach number. Besides this turbulent profile we also consider the

following profile:

$$f(r) = \begin{cases} \dfrac{m+2}{m}\left(1 - \left(\dfrac{r}{r_1}\right)^m\right), & 0 \leqslant r \leqslant r_1, \\ 0, & r_1 < r \leqslant r_2. \end{cases} \tag{32}$$

Also here the average of the profile function over the upstream pipe area equals unity. This profile is, for the m values that will be considered here, very close to a jet flow profile, see e.g. [29]. Figs. 9–16 show the experimental data of Ronneberger [1] for the downstream and upstream reflection and transmission

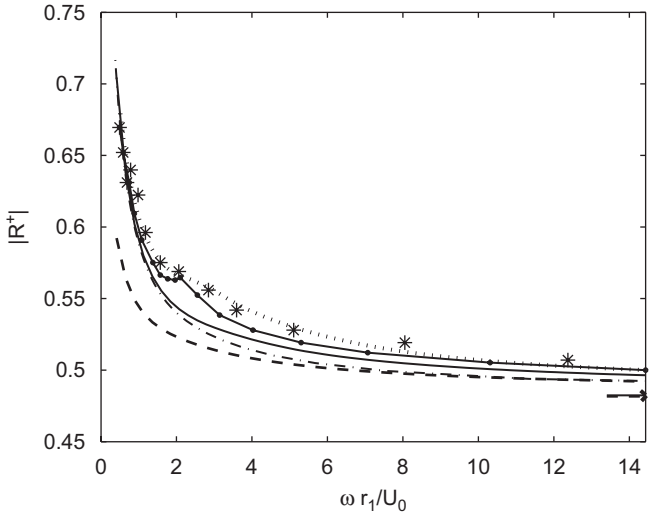

Fig. 9. Magnitude of the downstream reflection coefficient R^+ at an area expansion in a 2D cylindrical duct. Helmholtz number on upstream duct radius: $k_0 r_1 = 0.227$, expansion ratio: $\eta = 0.35$. $*$ markers: experimental data Ronneberger [1]. Multimodal method calculations ($N_1 = 100$, $N_2 = 169$) for: uniform mean flow (solid line), turbulent pipe flow, Eq. (30), with $m = 7$ (dashed line), and flow profile Eq.(32) with $m = 15$ (dotted line). Dash-dot line: result of simplified multimodal method by Aurégan [22,23]. Solid line with • markers: fit of Boij and Nilsson's result for the equivalent rectangular geometry [12,28]. Dashed arrow: quasi-steady limit without mean flow. Solid arrow: multimodal method result without mean flow.

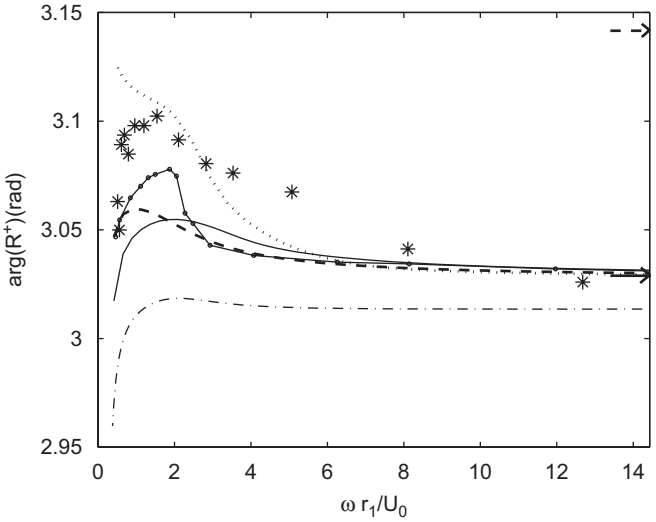

Fig. 10. Phase of the downstream reflection coefficient R^+ at an area expansion in a 2D cylindrical duct. Helmholtz number on upstream duct radius: $k_0 r_1 = 0.227$, expansion ratio: $\eta = 0.35$. Data indication as in Fig. 9.

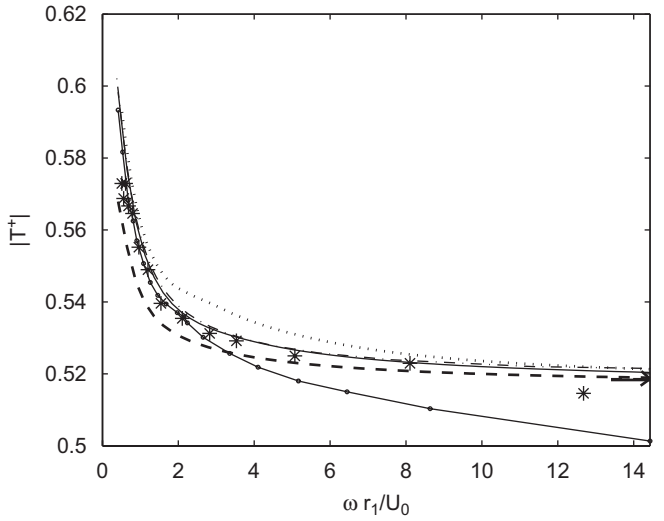

Fig. 11. Magnitude of downstream transmission coefficient T^+ at an area expansion in a 2D cylindrical duct. Helmholtz number on upstream duct radius: $k_0 r_1 = 0.227$, expansion ratio: $\eta = 0.35$. Data indication as in Fig. 9.

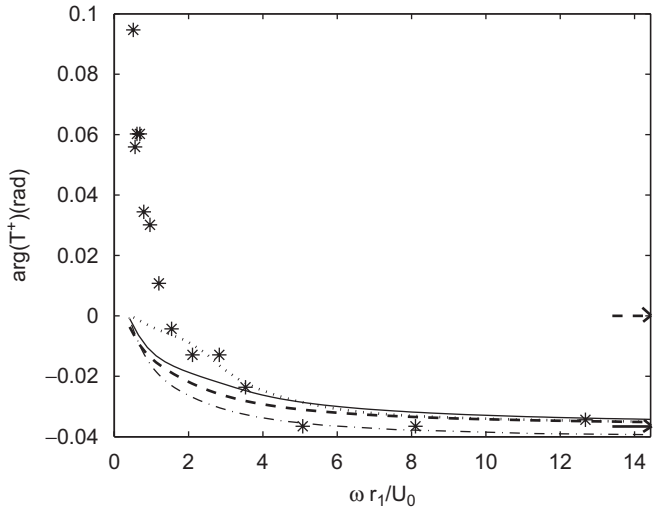

Fig. 12. Phase of downstream transmission coefficient T^+ at an area expansion in a 2D cylindrical duct. Helmholtz number on upstream duct radius: $k_0 r_1 = 0.227$, expansion ratio: $\eta = 0.35$. $*$ markers: experimental data Ronneberger [1]. Multimodal method calculations ($N_1 = 100$, $N_2 = 169$) for: uniform mean flow (solid line), turbulent pipe flow, Eq. (30), with $m = 7$ (dashed line), and flow profile Eq.(32) with $m = 15$ (dotted line). Dash-dot line: result of simplified multimodal method by Aurégan [22,23]. Dashed arrow: quasi-steady limit without mean flow. Solid arrow: multimodal method result without mean flow.

coefficients at the area expansion with the above given configuration. The results are plotted versus the Strouhal number $\omega r_1/U_0$. On basis of the representation in Ref. [1], the error in the magnitudes and phases is estimated at ± 0.01 and ± 0.04 ($\approx \pm 0.01\pi$), respectively, for the experimental data. The figures also show results of mode-matching calculations for cylindrical geometry with uniform mean flow (infinitely thin shear layer) as well as with the turbulent pipe flow profile, Eq. (30), with $m = 7$, and the jet flow profile of Eq. (32) with $m = 15$. These latter two non-uniform profiles are plotted in Fig. 17. The number of points in the mode-matching calculations is $N_1 = 100$ and $N_2 = 169$. For the downstream reflection and transmission coefficients also the results for an infinitely thin shear layer as obtained by the simplified multimodal method of Aurégan [22,23] and as obtained by Boij and Nilsson [12,28] for the equivalent rectangular geometry are shown.

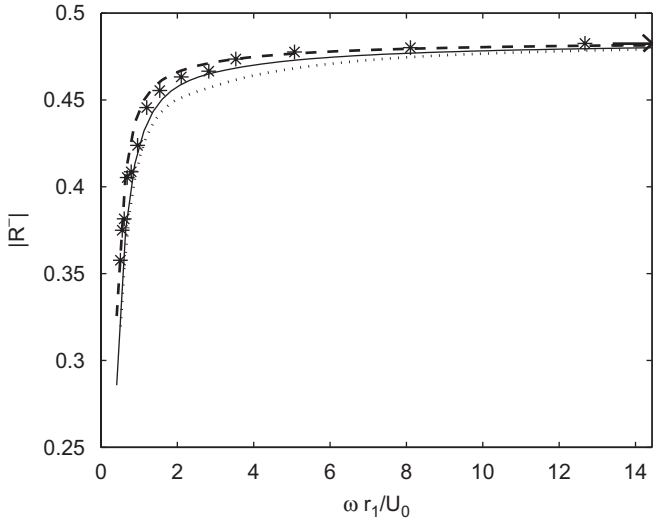

Fig. 13. Magnitude of upstream reflection coefficient R^- at an area expansion in a 2D cylindrical duct. Helmholtz number on upstream duct radius: $k_0 r_1 = 0.227$, expansion ratio: $\eta = 0.35$. $*$ markers: experimental data Ronneberger [1]. Multimodal method calculations ($N_1 = 100$, $N_2 = 169$) for: uniform mean flow (solid line), turbulent pipe flow, Eq. (30), with $m = 7$ (dashed line), and flow profile Eq.(32) with $m = 15$ (dotted line). Dashed arrow: quasi-steady limit without mean flow. Solid arrow: multimodal method result without mean flow.

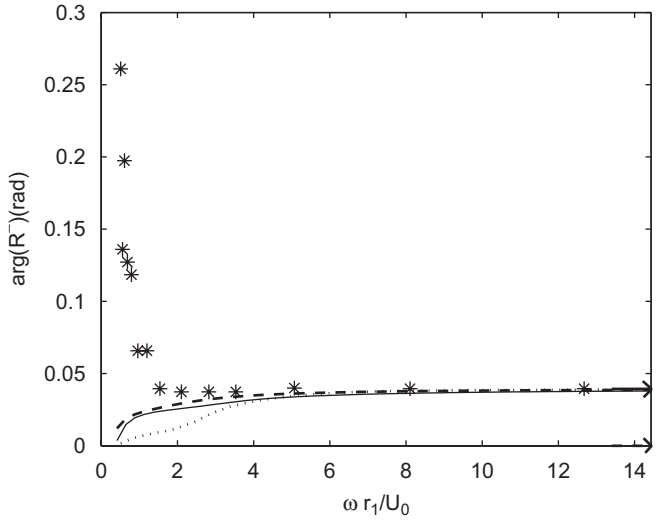

Fig. 14. Phase of upstream reflection coefficient R^- at an area expansion in a 2D cylindrical duct. Helmholtz number on upstream duct radius: $k_0 r_1 = 0.227$, expansion ratio: $\eta = 0.35$. Data indication as in Fig. 13.

The quasi-steady limit as well as the result obtained by the current multimodal method in absence of mean flow are indicated by the dashed and solid arrows, respectively.

The effect of a non-uniform mean flow compared to uniform mean flow on the magnitude of the reflection and transmission coefficients in the multimodal method is opposite for the turbulent pipe flow and the jet flow profile. The magnitudes of R^+, T^+ and T^- decrease when taking the turbulent profile compared to the uniform flow profile, whereas the magnitude of R^- increases. For the jet flow profile this is exactly opposite. Concerning the phase of the reflection and transmission coefficients the turbulent pipe flow profile and the jet flow profile qualitatively have the same effect compared to uniform flow for R^+ and T^-. For the phase of T^+

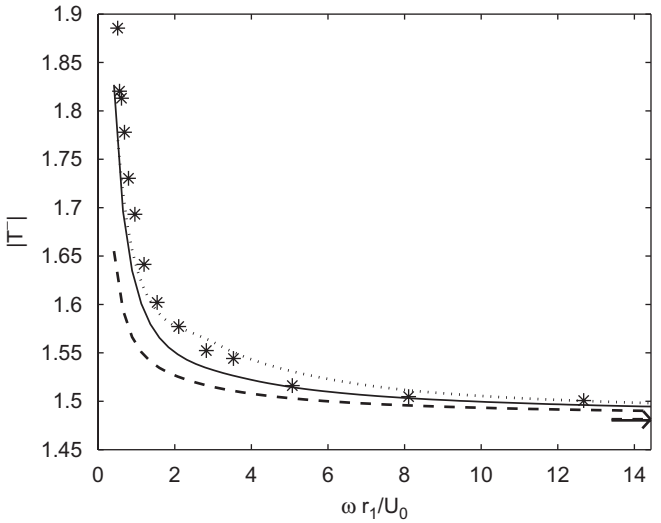

Fig. 15. Magnitude of upstream transmission coefficient T^- at an area expansion in a 2D cylindrical duct. Helmholtz number on upstream duct radius: $k_0 r_1 = 0.227$, expansion ratio: $\eta = 0.35$. Data indication as in Fig. 13.

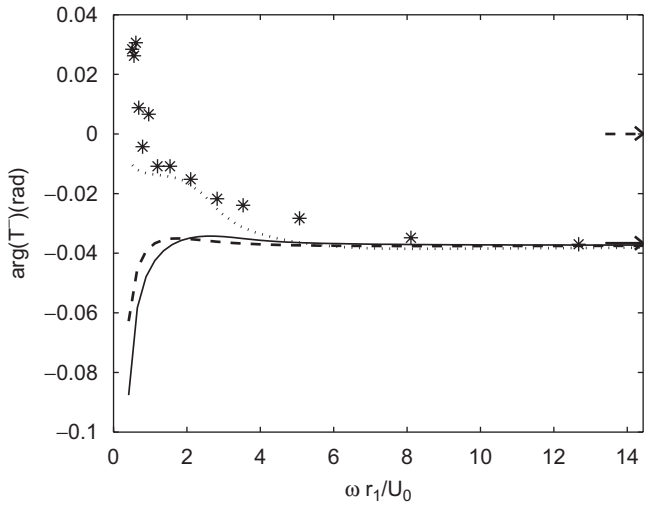

Fig. 16. Phase of upstream transmission coefficient T^- at an area expansion in a 2D cylindrical duct. Helmholtz number on upstream duct radius: $k_0 r_1 = 0.227$, expansion ratio: $\eta = 0.35$. Data indication as in Fig. 13.

and R^- the effect is opposite. The flow profile which gives the best fit between mode-matching calculations and experimental data varies for the different reflection and transmission coefficients. For the magnitude of R^+ the jet flow profile clearly gives a better resemblance with experimental data compared to the uniform profile, whereas the turbulent pipe flow profile gives a worse prediction. For the phase of R^+ the jet flow profile seems to give better results for some Strouhal numbers, however, the turbulent pipe flow profile gives the best results for very low Strouhal. The experimental data for the magnitude of the downstream transmission coefficient T^+ is between the mode-matching results for uniform flow and turbulent pipe flow. The jet flow profile gives worse resemblance compared to uniform flow. The same as for T^+ is more or less seen for the upstream reflection coefficient R^-. Although here, clearly, the turbulent pipe flow profile gives better resemblance with experiments for the magnitude of R^- at Strouhal numbers larger than 1. The jet flow profile gives a worse

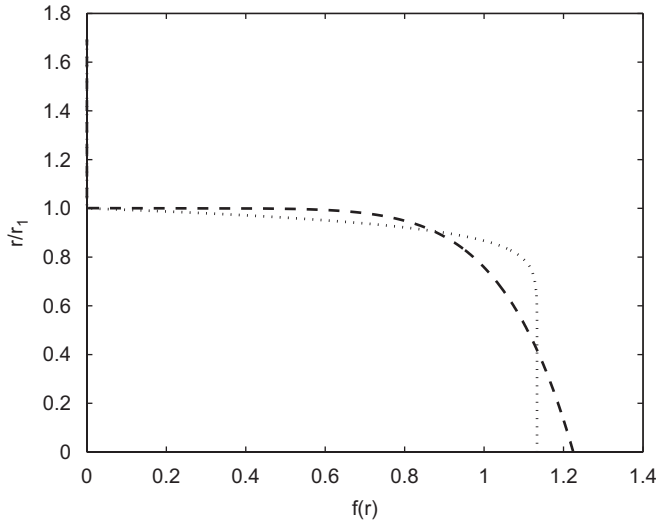

Fig. 17. Non-uniform flow profiles as used in the multimodal method calculations, Figs. 9 through 16. Dashed line: turbulent pipe flow, Eq. (30), with parameter $m = 7$. Dotted line: flow profile function, Eq. (32), with $m = 15$.

prediction for both magnitude and phase of R^-. For the upstream transmission coefficient T^- the results for the jet flow profile are most consistent with experimental data, both for magnitude and phase. The turbulent pipe flow profile gives a worse prediction at least for the magnitude of T^- compared to the other profiles. Thus, for the magnitudes of R^+ and T^- the calculations with the jet flow profile give a better prediction than those with uniform flow. The calculations with the turbulent pipe flow give a worse prediction. For the magnitudes of T^+ and R^- the calculations with the turbulent pipe flow profile give a slightly better resemblance with experiments than those with uniform flow. The jet flow profile clearly gives a worse prediction in these cases. For the phase of the reflection and transmission coefficients the result of the calculations are most consistent with experiments for large Strouhal number. Here, the results for the different flow profiles coincide. At low Strouhal numbers the deviation in phase between experiments and calculations is larger. The jet flow profile seems to give a better prediction in this range than the uniform flow profile, except for R^-. At high Strouhal numbers the results obtained for the different flow profiles coincide. For the uniform flow profile, the (infinitely thin) shear layer is always unstable. For the non-uniform profiles this hydrodynamic instability however vanishes at sufficiently high Strouhal number (in this case at approximately $\omega r_1/U_0 = 12$). This means that for the area expansion the effect of the hydrodynamic instability, and in particular the non-vanishing of it for infinitely thin shear layers, is negligible for high Strouhal numbers. This conclusion was also drawn by Boij and Nilsson [28] and Howe [39]. Note that calculations with the jet flow profile, Eq. (32), with other, lower, values of the profile parameter m than used here, yielding a thicker boundary layer and shear layer, can be found in Ref. [21]. Qualitatively the effect on the scattering coefficients compared to the case of uniform flow is the same for these lower m values as observed here for $m = 15$. Only, quantitatively, the deviation from the case of uniform flow and from the experimental data is larger for lower values of m. It also has to be noted here that for the turbulent pipe flow profile with profile parameter $m = 7$ as used above the displacement thickness δ_1 and momentum thickness δ_2 are $\delta_1/r_1 = 0.10$ and $\delta_2/r_1 = 0.08$, respectively, whereas for the used jet flow profile with profile parameter $m = 15$ these values are $\delta_1/r_1 = 0.06$ and $\delta_2/r_1 = 0.03$, respectively. Furthermore, the results obtained by the current multimodal method for an infinitely thin shear layer are generally closer to experimental data than those obtained by the simplified multimodal method of Aurégan [22,23]. For the downstream reflection coefficient R^+ the results obtained by Boij and Nilsson [12,28] for the equivalent 2D rectangular geometry coincide slightly better with experiments than the multimodal method results for uniform mean flow in 2D cylindrical geometry. This especially holds in the region, where the hump is observed. As mentioned above this hump is, however, a result of the 2D rectangular geometry they used.

4. Conclusion

The scattering of sound at a sudden area expansion in a duct carrying mean (sheared) flow has been modelled with a multimodal analysis method. In this method the pressure and velocity disturbance fields are solved as an expansion of eigenmodes both upstream and downstream of the area expansion. Mode matching at the area discontinuity, i.e. demanding continuity of the acoustic mass and momentum flux, subsequently gives the scattering matrix, which relates all modes.

Calculations have been done for both 2D rectangular and 2D cylindrical geometry and for uniform mean flow (infinitely thin shear layer) as well as non-uniform mean flow. Scattering results for the 2D rectangular geometry with uniform flow are compared to results of the model of Boij and Nilsson [12,28]. Especially for the downstream reflection coefficient of plane waves good agreement is found. Also calculations for a 2D cylindrical duct with uniform flow with the same area expansion ratio are carried out in order to test the scaling rule which is proposed by Boij and Nilsson [12] for comparison of 2D rectangular calculations with experiments is cylindrical geometry. Generally, the suggested scaling is found to be useful for the magnitudes of the scattering coefficients. However, around a Strouhal number of about unity, specific behaviour of the scattering coefficients is observed depending on the ratio of duct heights, respectively, the ratio of duct radii. Since for given area expansion ratio the ratios of duct heights and ratio of duct radii is not the same, a deviation between calculations for the two geometries can be seen. The mentioned behaviour in the scattering coefficients is closely related to the behaviour of the unstable hydrodynamic modes and the first higher-order evanescent acoustic modes [32].

Results for the plane wave scattering coefficients as calculated by the multimodal method are fairly consistent with experimental data from literature [1] for an area expansion in a cylindrical pipe. Results obtained by taking a uniform flow profile (infinitely thin shear layer) already give a slightly better prediction of the experimental results than the simplified multimodal method of Aurégan [22,23]. Furthermore, taking a turbulent pipe flow profile in the calculations yields a better agreement compared to a uniform flow profile for the downstream transmission and the upstream reflection coefficient. However, worse agreement is seen for the upstream transmission and downstream reflection coefficient. On the contrary, compared to uniform flow a non-uniform jet flow profile, which represents more a typical shear layer flow downstream of the expansion, gives worse agreement for the downstream transmission and the upstream reflection coefficient, whereas prediction for the other coefficients improves. As the turbulent pipe flow profile would best resemble the flow upstream of the expansion, whereas the jet flow profile would best resemble the flow downstream of the expansion, a physical argument is present for having employed these two profiles in the present model calculations. A related physical explanation may thus be present for the fact that different plane wave scattering coefficients are predicted better by either employing a turbulent pipe flow- or a jet flow profile. However, as the scattering at the expansion is complex, i.e. all modes propagating towards and away from the expansion are related, this will be not straightforward.

Acknowledgments

The authors would like to thank Pierre Moussou for his contribution in the work of Phillipe Testud. This research was financially supported by the Dutch Technology Foundation STW.

References

[1] D. Ronneberger, Theoretische und experimentelle Untersuchung der Schall-ausbreitung durch Querschnittssprünge und Lochplatten in Strömungskanälen, Abschlußbericht Ro 369/11, 12, 14; Drittes Physikalisches Institut der Universität Göttingen, 1987.

[2] J. Miles, The reflection of sound due to a change in cross section of a circular tube, *Journal of the Acoustical Society of America* 16 (1) (1944) 14–19.

[3] J. Kergomard, A. Garcia, Simple discontinuities in acoustic waveguides at low frequencies: critical analysis and formulae, *Journal of Sound and Vibration* 114 (3) (1987) 465–479.

[4] D. Ronneberger, Experimentelle Untersuchungen zum akustischen Reflexions-faktor von unstetigen Querschnittsänderungen in einem luftdurchströmten Rohr, *Acustica* 19 (1967/68) 222–235.

[5] R.J. Alfredson, P.O.A.L. Davies, Performance of exhaust silencer components, *Journal of Sound and Vibration* 15 (2) (1971) 175–196.

[6] A. Cummings, Sound transmission at sudden area expansions in circular ducts, with superimposed mean flow, *Journal of Sound and Vibration* 38 (1975) 149–155.
[7] A. Cummings, H. Haddad, Sudden area changes in flow ducts: further thoughts, *Journal of Sound and Vibration* 54 (4) (1977) 611–612.
[8] R.F. Lambert, E.A. Steinbrueck, Acoustic synthesis of a flowduct area discontinuity, *Journal of the Acoustical Society of America* 67 (1) (1980) 59–65.
[9] F.C. Karal, The analogous acoustical impedance for discontinuities and constrictions of circular cross section, *Journal of the Acoustical Society of America* 25 (2) (1953) 327–334.
[10] P.O.A.L. Davies, Practical flow duct acoustics, *Journal of Sound and Vibration* 124 (1) (1988) 92–115.
[11] K.S. Peat, The acoustical impedance at discontinuities of ducts in the presence of a mean flow, *Journal of Sound and Vibration* 127 (1) (1988) 123–132.
[12] S. Boij, B. Nilsson, Reflection of sound at area expansions in a flow duct, *Journal of Sound and Vibration* 260 (3) (2003) 477–498.
[13] M.C.A.M. Peters, Aeroacoustical Sources in Internal Flows, PhD Thesis, Technische Universiteit Eindhoven, NL, 1993, ISBN 90-386-0282-0.
[14] M.C.A.M. Peters, A. Hirschberg, A.J. Reijnen, A.P.J. Wijnands, Damping and reflection coefficient measurements for an open pipe at low Mach and low Helmholtz numbers, *Journal of Fluid Mechanics* 256 (1993) 499–534.
[15] S. Allam, M. Åbom, Investigation of damping and radiation using full plane wave decomposition in ducts, *Journal of Sound and Vibration* 292 (2006) 519–534.
[16] R.M. Munt, The interaction of sound with a subsonic jet issuing from a semi-infinite cylindrical pipe, *Journal of Fluid Mechanics* 83 (4) (1977) 609–640.
[17] R.M. Munt, Acoustic transmission properties of a jet pipe with subsonic flow: 1. The cold jet reflection coefficient, *Journal of Sound and Vibration* 142 (3) (1990) 413–436.
[18] S.W. Rienstra, A small Strouhal number analysis for acoustic wave-jet flow-pipe interaction, *Journal of Sound and Vibration* 86 (4) (1983) 539–556.
[19] A.M. Cargill, Low frequency acoustic radiation from a jet pipe—a second order theory, *Journal of Sound and Vibration* 83 (3) (1982) 339–354.
[20] G.C.J. Hofmans, Vortex Sound in Confined Flows, PhD Thesis, Technische Universiteit Eindhoven, NL, 1998, ISBN 90-386-0697-4.
[21] P. Testud, Aeroacoustics of Orifices in Confined Flow: Whistling and Cavitation, PhD Thesis, Université du Maine, Le Mans, France, 2006.
[22] Y. Aurégan, Comportement aero-acoustique basse-frequence d'une expansion, 14ème Congrès Français de Mécanique, No. 451, Toulouse, 1999.
[23] Y. Aurégan, A. Debray, R. Starobinski, Low frequency sound propagation in a coaxial cylindrical duct: application to sudden area expansions and to dissipative silencers, *Journal of Sound and Vibration* 243 (3) (2001) 461–473.
[24] R.N. Starobinski, E.I. Ioudine, On the low frequency sound propagation in a lined duct, *Journal of Acoustic*, *Science Academy of CCCP* XVIII (1972) 115–118.
[25] B. Nilsson, O. Brander, The propagation of sound in cylindrical ducts with mean flow and bulk reacting lining—III. Step discontinuities, *IMA Journal of Applied Mathematics* 27 (1981) 105–131.
[26] B. Nilsson, O. Brander, The propagation of sound in cylindrical ducts with mean flow and bulk reacting lining—IV. Several interacting discontinuities, *IMA Journal of Applied Mathematics* 27 (1981) 263–289.
[27] I.D.J. Dupère, A.P. Dowling, The absorption of sound near abrupt axisymmetric area expansions, *Journal of Sound and Vibration* 239 (4) (2001) 709–730.
[28] S. Boij, B. Nilsson, Scattering and absorption of sound at flow duct expansions, *Journal of Sound and Vibration* 289 (3) (2006) 577–594.
[29] A. Michalke, The influence of the vorticity distribution on the inviscid instability of a free shear layer, *Fluid Dynamics Transactions* 4 (1969) 751–760.
[30] Y. Aurégan, M. Leroux, V. Pagneux, Measurement of liner impedance with flow by an inverse method, *10th AIAA/CEAS Aeroacoustics Conference* (2004) AIAA 2004-2838.
[31] G. Kooijman, Y. Aurégan, A. Hirschberg, Orifice impedance under grazing flow, modal expansion approach, *11th AIAA/CEAS Aeroacoustics Conference* (2005) AIAA 2005-2857.
[32] G. Kooijman, Acoustical Response of Shear Layers, PhD Thesis, Eindhoven University of Technology, NL, 2007, ISBN-10: 90-386-2182-5, ISBN-13: 978-90-386-2182-1.
[33] M. Leroux, Propagation Acoustique en Conduit Traité: Influence de l'Ecoulement sur la Propagation Avec Impédance de Paroi, PhD Thesis, Université du Maine, Le Mans, France, 2005.
[34] R.J. Briggs, *Electron–Stream Interaction with Plasmas*, MIT Press, Cambridge, MA, 1964.
[35] A. Bers, Space–time evolution of plasma instabilities—absolute and convective, in: A.A. Galeev, R.N. Sudan (Eds.), *Handbook of Plasma Physics, Vol. 1, Basic Plasma Physics*, North-Holland Publishing Company, Amsterdam, 1983 ISBN 0-444-86645-0.
[36] D.G. Crighton, F.G. Leppington, Radiation properties of the semi-infinite vortex sheet: the initial-value problem, *Journal of Fluid Mechanics* 64 (2) (1974) 393–414.
[37] S.W. Rienstra, N. Peake, Modal scattering at an impedance transition in a lined flow duct, *11th AIAA/CEAS Aeroacoustics Conference* (2005) AIAA 2005-2852.
[38] H. Schlichting, *Boundary Layer Theory*, seventh ed., Springer, Berlin, 1979 ISBN 0-07-055334-3.
[39] M.S. Howe, Attenuation of sound in a low Mach number nozzle flow, *Journal of Fluid Mechanics* 91 (1979) 209–229.